



Contents lists available at ScienceDirect

Arabian Journal of Chemistry

journal homepage: www.ksu.edu.sa

Turning dextran into antibacterial fibers: Quaternary ammonium salt for antibacterial treatment and wound healing

Guangyu Pan^{a,b,1}, Qin Wang^{a,b,1}, Hangxing Ding^{a,b,1}, Jianbin Deng^c, Shiqi Gao^c, Liping Wang^{a,b,d,*}

^a School of Intelligent Medicine and Biotechnology, Guilin Medical University, Guilin 541199, Guangxi, China

^b Key Laboratory of Biochemistry and Molecular Biology, Guilin Medical University, Guilin 541199, Guangxi, China

^c School of Pharmacy, Guilin Medical University, Guilin 541199, Guangxi, China

^d Guangxi Engineering Research Center of Digital Medicine and Clinical Translation, Guilin Medical University, Guilin 541199, Guangxi, China

ARTICLE INFO

Keywords:

Antimicrobial materials
Quaternary ammonium salt antibacterial fibers
Staphylococcus aureus
Methicillin-resistant

ABSTRACT

This study aims to develop new quaternary ammonium salt-based antimicrobial materials with good biocompatibility, biosafety, and strong antimicrobial properties that promote wound healing in infected wounds. First, four new quaternary ammonium salt antibacterial fibers (QASAF) are constructed: QASAF-C12, QASAF-C14, QASAF-C16, and QASAF-C18, with varying carbon chain lengths of C12, C14, C16, and C18, respectively. Then, their structure is characterized by proton nuclear magnetic resonance (NMR) analysis and their hemolytic and cytotoxic properties are also investigated. QASAFs are then evaluated for *in vivo* and *in vitro* antimicrobial performance against Staphylococcus aureus (*S. aureus*) and methicillin-resistant Staphylococcus aureus (MRSA). Finally, the effect of QASAF on promoting wound healing in infected wounds is evaluated using mouse wound models infected with *S. aureus* and MRSA. The obtained results suggest that QASAF is non-toxic to cells in the 25–125 µg/mL concentration range, is slightly hemolytic, has good biocompatibility, and has a biosafety profile. QASAF-C18 shows the best antibacterial performance against *S. aureus* with significant pro-healing effects on infected wounds. QASAF-C12 exhibits the best antibacterial performance against MRSA with significant pro-healing effects. The novel quaternary ammonium-based antimicrobial material provides a reference for developing antimicrobial and biocompatible wound dressings.

1. Introduction

Millions worldwide die yearly from malignant bacterial infections (Brumfitt and Hamilton-Miller, 1989, Becker et al., 2017, Minozzi et al., 2021). Currently, bacterial illnesses are commonly treated with antibiotics. Since antibiotic use has increased, bacterial resistance has risen considerably. Up to 700,000 drug-resistant bacterial illnesses occur yearly (C., 2017). In recent years, the research on antibacterial materials has been mainly divided into metal–organic frameworks (MOFs) (Shen et al., 2020), transition metals (Qi et al., 2020), organic materials (Saidin et al., 2021), carbon-based (Mann et al., 2021), and precious metal materials (Zhou et al., 2021). MOF antibacterial materials possess excellent antibacterial properties; however, biocompatibility problems still exist.

Although transition metal compounds exhibit high physiological stability, their manufacturing is difficult, and biosafety needs improvement (Qiao et al., 2019, Yuan et al., 2019). On the other hand, organic materials can be flexibly processed and are biocompatible; however, their synthesis process is complicated (Diven et al., 1996, Linsley et al., 2015). Although carbon-based materials have the advantages of adjustable parameters, good thermal stability, and low cost, they have high toxicity and poor antibacterial properties (Qian et al., 2018, Lee et al., 2020). Therefore, improving blood compatibility and biocompatibility is an urgent challenge for developing new antimicrobial materials.

Quaternary ammonium salts (QAS) are the cationic antibacterial agent penetrating bacterial cells, destroying electrolytes, and damaging cell membranes, thereby playing a bactericidal role (Rajkowska et al.,

Peer review under responsibility of King Saud University.

* Corresponding author at: Guangxi Engineering Research Center of Digital Medicine and Clinical Translation, School of Intelligent Medicine and Biotechnology, Guilin Medical University, Guilin 541199, Guangxi, China.

E-mail address: lipingwang0206@163.com (L. Wang).

¹ These authors contributed equally to this work.

<https://doi.org/10.1016/j.arabjc.2024.105771>

Received 12 June 2023; Accepted 30 March 2024

Available online 7 April 2024

1878-5352/© 2024 The Author(s). Published by Elsevier B.V. on behalf of King Saud University. This is an open access article under the CC BY-NC-ND license (<http://creativecommons.org/licenses/by-nc-nd/4.0/>).

2016). The cationic quaternary ammonium ions in the QAS structure can be anchored on the polymer chain (Wiarachai et al., 2012, Zhao et al., 2020, Choi et al., 2021). The antibacterial effect of QAS is enhanced with increasing alkyl chain length on the nitrogen atom in the quaternary ammonium salt (Gottenbos et al., 2002). Normally, the best antibacterial effect is observed for the chain length of 12–18 carbon atoms (Vereshchagin et al., 2021). QAS exhibits high antibacterial efficiency; however, proteins and red blood cells in damaged tissues easily bind to QAS (Pérez et al., 2009, Jiao et al., 2017). Therefore, the blood compatibility and biocompatibility of QAS-based materials are still insufficient. Therefore, improving blood compatibility and biocompatibility is the main challenge in developing QAS antibacterial materials.

Dextran is produced from sugars or chemical synthesis under bacterial action (Wangpaiboon et al., 2020). Dextran is rich in hydroxyl groups and readily mixes with drugs and proteins via non-covalent or covalent interactions (Del Bino et al., 2022). Due to its good physical and chemical properties and non-toxicity, dextran has become a potential drug macromolecular carrier. In addition, it improves blood compatibility and affects coagulation homeostasis, such as inhibition of platelet activation and red blood cell formation (Zeerleder et al., 2002, Neu et al., 2008, Ferrer et al., 2013). Yang et al. reported enhanced thermoplastic polyurethane materials' blood compatibility by surface immobilizing chitosan and dextran sulfate (Usman et al., 2016). Polyvinyl alcohol/dextran hydrogel reported by Alexandre et al. significantly lowered the hemolysis index since Dextran protects red blood cells, thereby improving blood compatibility and biocompatibility (Alexandre et al., 2014, Gharibi et al., 2019). Therefore, combining the advantages of QAS and Dextran, a hypothesis is proposed: Synthesizing antimicrobial materials containing dextran backbone by covalently linking QAS

can improve the blood compatibility, biocompatibility, and antimicrobial properties of QAS-based antimicrobial materials.

Different types of quaternary ammonium salt antimicrobial fibers (QASAF) are constructed. The synthesis of QASAF and the *in vitro* and *in vivo* antibacterial mechanisms are described in Fig. 1. First, Epoxypropyl Alkyl Dimethyl Ammonium Bromide (EPADMAB) with different carbon chain lengths is synthesized. Then, EPADMAB is grafted on dextran to obtain QASAF. The chemical structure of QASAF is characterized to evaluate its cytotoxicity, hemolysis, and biosafety and to investigate the *in vivo* and *in vitro* antibacterial properties against *S. aureus* and MRSA. Finally, the pro-healing effect of as-synthesized fibers on infected wounds in mice is evaluated. Obtained results serve as a guide for making antibacterial and wound-healing dressings.

2. Materials and methods

2.1. Ethical approval

All experiments were performed under the guidelines of the Animal Experimentation Ethics Committee of Guilin Medical University (approval No. GLMC202103275).

2.2. Preparation

2.2.1. Synthesis of quaternary ammonium salt intermediates with different carbon chains

The quaternary ammonium salt intermediate (QASI) with a carbon chain length of C12 was synthesized according to previous literature (Deng et al., 2021) using N, N-dimethyl dodecyl amine (Xinguang

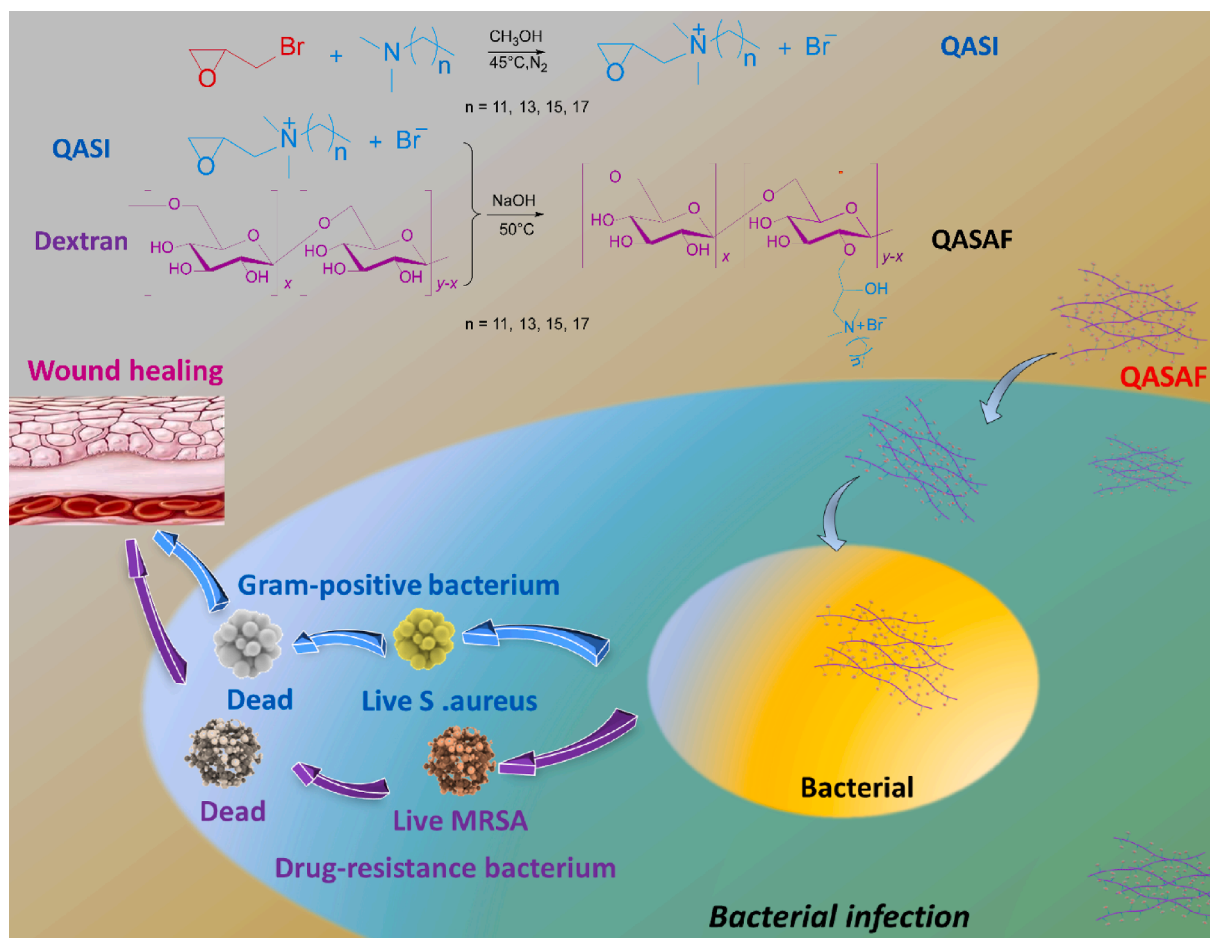


Fig. 1. Synthesis of antimicrobial fibers and *in vitro* and *in vivo* mechanisms.

Chemical Engineering Co., Ltd., Shanghai, China) and epoxy bromopropane (Aladdin Co., Ltd., Shanghai, China). The N, N-dimethyl dodecyl amine (9.8085 g), and methanol (5 mL) were added to a 100 mL two-necked round-bottom flask. Then, a mixture of 5 mL methanol (Aladdin Co. Ltd., Shanghai, China) and 7.2012 g epoxybromopropane (Aladdin Co. Ltd., Shanghai, China) was added dropwise to the above flask, and the reaction was carried out for 2 h at 45 °C under nitrogen atmosphere. Methanol was evaporated using a rotary evaporator (N-1300, Shanghai Eyela Co., Ltd., Shanghai, China) under a vacuum. After recrystallizing five times with ethyl acetate (Sinopharm Reagent Co., Ltd., Shanghai, China), the finished product was vacuum dried at 40 °C for 24 h. The product was marketed as QASI-C12 (Fig. 2A).

The quaternary ammonium salt intermediates with carbon chain lengths of C14, C16, and C18 were synthesized using relevant precursors; N, N-dimethyltetradecylamine, N, N-dimethylhexadecylamine, N, N-dimethyl octadecylamine, respectively. The synthesized quaternary ammonium salt intermediates were named QASI-C14, QASI-C16, and QASI-C18, respectively, and then characterized by ¹H NMR.

2.2.2. Synthesis of antibacterial fibers of quaternary ammonium salts

The quaternary ammonium salt antibacterial fiber (QASAF) with different carbon chains was synthesized using a previously reported method (Yu et al., 2022). The synthetic route for QASAFs is shown in Fig. 2B. Briefly, 4.0 g dextran (Aladdin) was dissolved in 400 mL distilled water, 7.0 g QASI-C12 and 4.0 g NaOH was added, and the reaction was carried out at 50 °C for 3 h. Subsequently, the obtained mixture was cooled to room temperature, and neutralized with glacial acetic acid (Sinopharm Reagent Co., Ltd.). Finally, it was transferred to a 3.5 kD dialysis bag where it remained for 3 days in deionized water. Then, C12 quaternary ammonium salt antibacterial fiber was obtained by freeze-drying. Similarly, the QASAFs with different carbon chain lengths of C14, C16, and C18 were synthesized and named QASAF-C14, QASAF-C16, and QASAF-C18, respectively.

2.2.3. Nuclear magnetic resonance (NMR) analysis of QASI and QASAF

¹H NMR of each sample was carried out at room temperature using a 400 MHz NMR spectrometer (Bruker AVANCE III HD MRI, Bruker, Germany).

2.2.4. Zeta potential of QASI and QASAF

Zeta potentials of dextran, QASI, and QASAF were measured by a Malvern Nano ZS Zetasizer (Jiang et al., 2017, Xu et al., 2019) (Malvern Instruments, United Kingdom).

2.2.5. Hemolysis experiment of QASAF

1.0 mL of fresh blood was collected and placed in an EP tube containing an anticoagulant (Beijing Solarbio Science & Technology Co., Ltd, Beijing, China). Then, the fresh blood was centrifuged and washed thrice with Phosphate Buffered Saline (PBS) containing normal saline. 500 μL of red blood cell suspension was mixed with an equal volume of QASAF suspension at 25, 50, 75, 100, 125, and 150 μg/mL. Pure water was selected as the positive control (PC) group, whereas the negative control group (NC) was a PBS solution containing normal saline. The mixture was centrifuged after a 60-minute incubation at 37 °C. The supernatant was transferred to a 96-well plate to determine the relative hemolysis rate. The absorbance of samples was then tested at 590 nm, and the homolysis rate was calculated (Sun et al., 2021).

2.2.6. Cell culture

Human hepatocellular carcinoma cells (Hep G2) were derived from the School of Intelligent Medicine and Biotechnology of Guilin Medical University. The cell culture medium was DMEM medium (Gibco, US) containing streptomycin (100 μg/mL), penicillin (100 U/mL), and fetal bovine serum (10 %). The specific operation was as follows: Hep G2 cells were cultured in a constant temperature cell incubator at 37 °C (BPH-9082, Shanghai Yiheng Technology Instrument Co., Ltd., Shanghai, China) containing carbon dioxide (5 %). The medium was switched every other day. Cell passage, seed plate, cryopreservation, and all the following experiments were performed once the cell attachment density reached 80 %.

2.2.7. Cytotoxicity assay

The cytotoxicity of different QASAFs was determined by MTT assay (Zhang et al., 2016). Hep G2 cells in the logarithmic growth phase were seeded in 96-well plates at a density of 5×10^4 cells per well and cultured in an incubator for 24 h. DMEM's medium containing 25, 50, 75, 100, and 125 μg/mL of QASAF replaced the solution in the original hole and was cultured in the incubator for another 24 h. 10 μL MTT (5 mg/mL) solution (Sigma Co., Ltd., Shanghai, China) was added to each well. Cultured in the incubator for 4 h. After removing the solution from each 96-well plate hole, 150 μL of DMSO was added to each hole. After shaking for 10 min, the absorbance of the lysate was measured at 490 nm by a microplate reader (Multiskan FC, Jiangsu Science Equipment Co., Ltd., Jiangsu, China) to calculate the relative cell viability.

The antibacterial growth curve was determined by a previously reported method (Zhang et al., 2016). In 96-well plates, 80 μL of normal saline was added to each well, and 10 μL QASAF samples with different

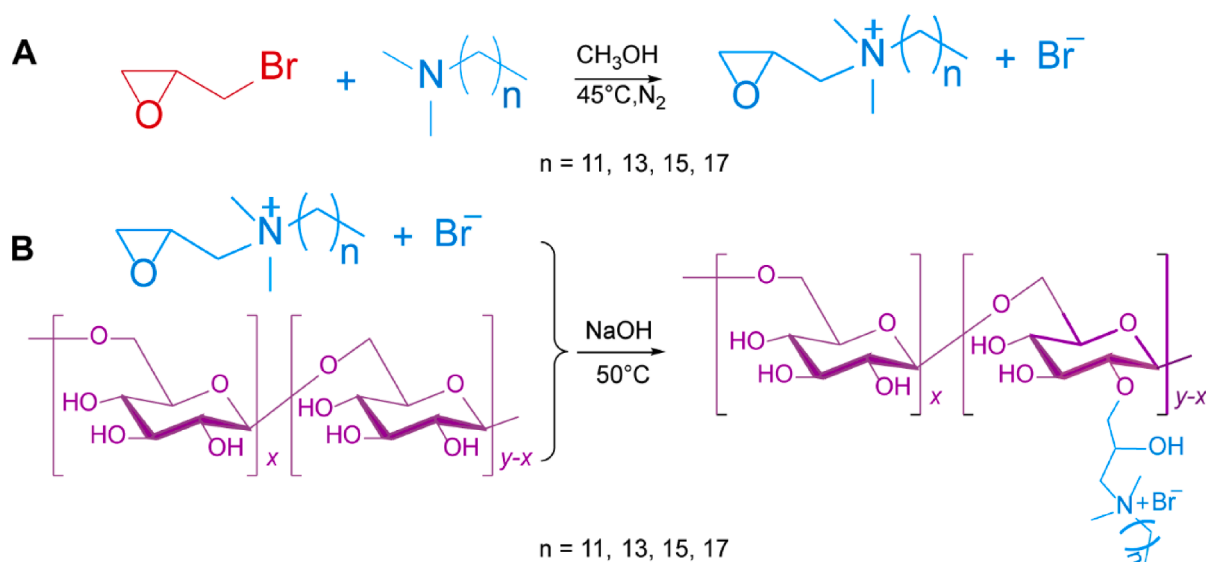


Fig. 2. (A) Synthesis route of each quaternary ammonium salt intermediate (B) and antimicrobial fibers with different carbon chain lengths.

concentration gradients were added to each well. After mixing, 10 μL of bacterial solution with OD600 = 0.5 was added to each well and incubated in a shaker (37°C, 180 rpm) for 10 min (Zhang et al., 2016). After adding 10 μL LB (10 \times) broth liquid medium, the OD600 was measured at 0, 2, 4, 6, 8, 10, 12, 24, 36, and 48 h using a microplate reader.

2.2.8. Determination of minimal inhibitory concentration

Minimal inhibitory concentration (MIC) is determined according to a previously reported reference (Zhang et al., 2016). The OD600 = 0.5 bacterial suspensions were diluted 10 times with normal saline. 80 μL of normal saline was added to each well of 96 well plate before adding 10 μL of QASAF samples with various concentration gradients was filled with and thoroughly mixed. After adding 10 μL of a diluted bacterial solution, the mixture was incubated in a shaker (37 °C, 180 rpm) for 10 min. The bacteria were cultured in a 37 °C thermostatic shaker (180 rpm) for 18 h after adding 10 μL LB broth liquid medium (10 \times). Then, 10 μL CCK-8 solution (Shanghai Dongren Technology Co., Ltd, Shanghai, China) was added to each well. The mixture was shaken for 10 min, and absorption was measured at 450 nm. Finally, the inhibitory effects of various doses of QASAF on bacteria were assessed from the absorption value.

2.2.9. Plate coating

400 μL normal saline and 50 μL QASAF samples were added to the EP tube. After mixing, 50 μL of bacterial solution with OD600 = 0.5 was added, and the mixture was placed in a thermostatic oscillator at 37 °C (180 rpm) for 10 min. 50 μL of the sample was taken from each tube and added dropwise to the LB agar plate petri dish, and the glass coating rod was used for coating. The plate was inverted and placed in a 37 °C constant temperature incubator for 18 h. Finally, photos were taken, and the number of colonies was counted.

2.2.10. Mice epidermal infection

Female Kunming mice (weighing 25–30 g) were anesthetized by intraperitoneal injection of 0.94 % sodium pentobarbital (Aladdin Co. Ltd, Shanghai, China). Next, a subcutaneous injection of 100 μL OD600 = 1.0 *S. aureus* and MRSA was done for 2 days to complete the epidermal *S. aureus* infection and MRSA infection models. 24 model mice infected with *S. aureus* were randomly divided into 2 groups of 12 each: the control group and the QASAF-C12 group. Similarly, 24 MRSA-infected model mice were randomly divided into 2 groups, the control, and QASAF-C12 groups, each of 12 mice.

On the 3rd and 4th days, 100 μL PBS and QASAF-C12 were subcutaneously injected at the infected site in the control and experimental groups, respectively. All mice were sacrificed on day 5, and each mouse's heart, liver, spleen, lung, kidney, and subcutaneous infected tissues were collected. Obtained samples were immersed in 4 % paraformaldehyde (Aladdin Co. Ltd, Shanghai, China) solution and sent to the Department of Pathology, Affiliated Hospital of Guilin Medical University for pathological analysis. Hematoxylin (H) and Zhuhai Besso Biotechnology Co., Ltd., Guangdong, China (Eosin, E) were used to stain the sections, and H&E stained pathological sections were photographed. After weighing the collected subcutaneous infected tissues, normal saline was added at 10 mg/mL (tissue weight/normal saline volume), and 5–6 pieces (1 m diameter) were added.

2.2.11. Wound healing in mice

Female Kunming mice (weighing 25–30 g) were anesthetized by intraperitoneal injection of 0.94 % pentobarbital sodium. A sharp stainless steel punch (8 mm in diameter) and stainless steel scissors were used to remove the skin and hair to obtain a wound of about 8 mm in diameter.

The *S. aureus* or MRSA suspension 100 μL (concentration of 1 \times 10⁸ CFU/mL) was slowly dropped to infect the wound and complete the model. The control groups and experimental mice were split randomly. PBS and QASAF were added to the wound on days 0, 1, and 2 of

infection, respectively. Photos were taken on days 0, 3, 6, 9, and 14, and Image J software was used to accurately measure the initial total wound area (A_0) and the total wound area (A_d). The wound healing rate (P , %) was calculated as follows (Guan et al., 2022):

$$P = (A_0 - A_d)/A_0 \times 100\% \quad (1)$$

The wounded tissues were collected and immersed in a 4 % paraformaldehyde solution on days 0, 3, 6, 9, and 14. H & E staining and Masson staining pathological sections were performed, and sections were photographed.

2.2.12. Statistical analyses

All data were expressed as the means \pm SD. One-way ANOVA performed multiple comparisons with Duncan's multiple range test post hoc analysis using SPSS version 13.0 software (IBM, Armonk, New York, USA). P values < 0.05 were considered statistically significant.

3. Results

3.1. Material properties of QASAF

The ¹H NMR spectra of the four QAS intermediates and the four antibacterial fibers were determined (Deng et al., 2021, Yu et al., 2022). After comparing the ¹H NMR spectra of QASI-C12 (Figure S1), QASI-C14 (Figure S2), QASI-C16 (Figure S3), QASI-C18 (Figure S4), and the raw materials, it was clearly revealed that the above four intermediate compounds were successfully synthesized. Similarly, the ¹H NMR spectra of the four antibacterial fibers (QASAF-C12, Figure S5; QASAF-C14, Figure S6; QASAF-C16, Figure S7; QASAF-C18, Figure S8) were compared with those of the QAS intermediates, which demonstrated that the four antibacterial fibers were also successfully synthesized.

The Zeta potential of dextran, QASI-C12, and QASAF-C12 is determined. The dextran polymer solution has a weak negative charge with a zeta potential of -1.5 ± 0.04 mv, while The Zeta potentials of QASI-C12, QASAF-C14, QASAF-C16 and QASAF-C18 are 21.30 ± 0.57 , 21.90 ± 0.80 , 38.40 ± 0.73 , and 39.10 ± 1.03 mV, respectively (Table 1). Chemical structure analyses of dextran and QASAF reveal that the dextran polymer is formed by glycosidic bonding between basic glucose units, and the molecules are uncharged or have a trace negative charge. In contrast, each quaternary ammonium salt intermediate and each QASAF molecule contain highly positively charged ammonium ions. Our results show that the positively charged QASI is successfully attached to the dextran backbone, generating positively charged quaternary ammonium antimicrobial fibers.

When the QASAF concentration is high, the hemolysis rate is < 5 %. The hemolysis rate of QASAF is lower in the effective inhibitory concentration range (Fig. 3A), indicating that QASAF is slightly hemolytic at higher concentrations, demonstrating good biosafety.

The inhibitory activity of QASAFs' different concentrations on Hep G2 cells is determined by MTT assay. The survival rate of Hep G2 cells is > 85 % (>70 %, no cytotoxicity (Xi et al., 2019)) at the 25–125 $\mu\text{g}/\text{mL}$ concentration range (Fig. 3B), suggesting that QASAF has good biocompatibility. Electron micrographs are taken for Hep G2 cells treated with QASAF at 125 $\mu\text{g}/\text{mL}$ concentration. Compared with the control group, there is no significant difference in the growth status and

Table 1
Zeta potential of Dextran, QASAF-C12, QASAF-C14, QASAF-C16 and QASAF-C18.

Sample	Zeta potential (mv)
Dextran	-1.5 ± 0.04
QASAF-C12	21.3 ± 0.57
QASAF-C14	21.9 ± 0.80
QASAF-C16	38.4 ± 0.73
QASAF-C18	39.1 ± 1.03

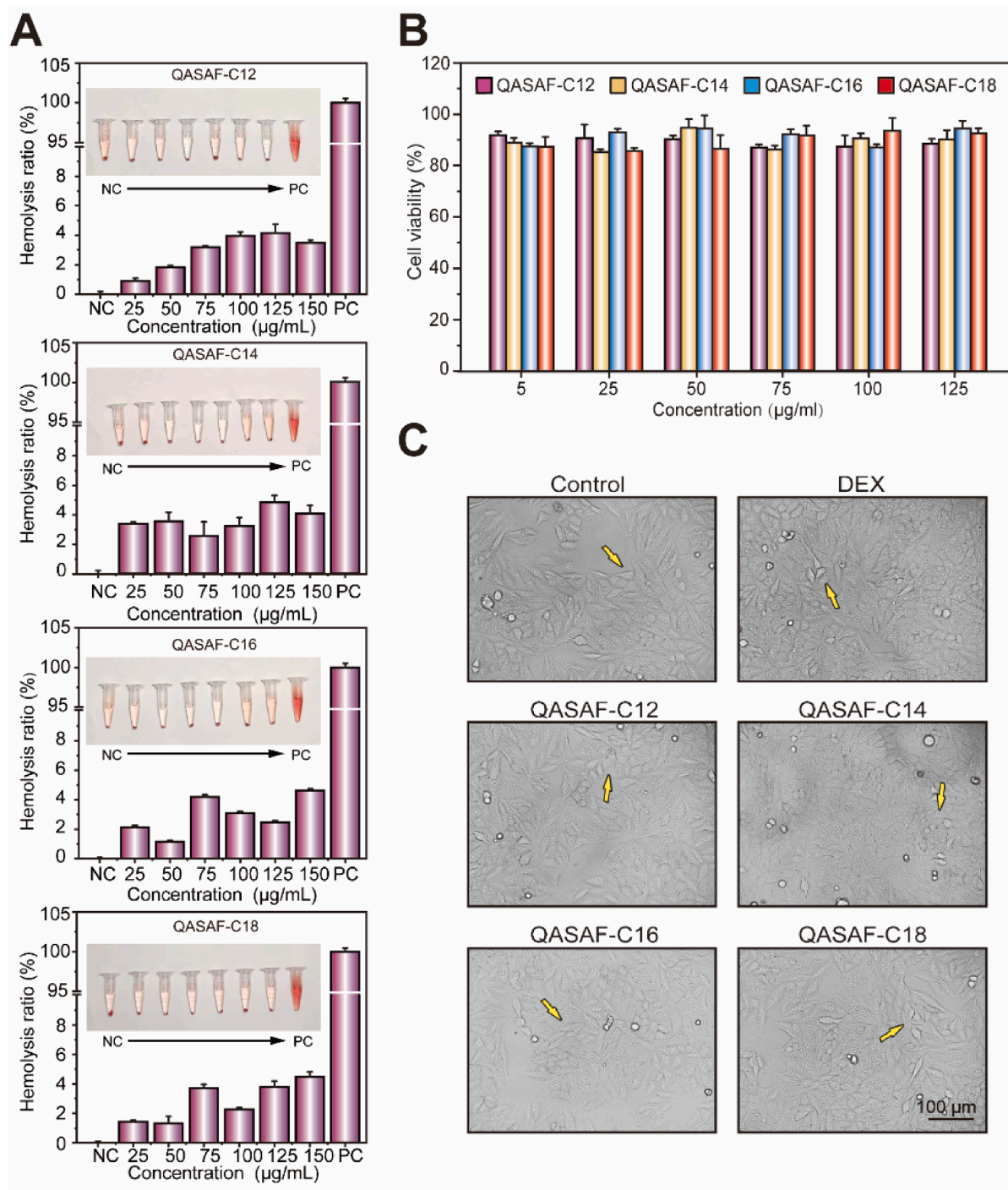


Fig. 3. (A) Hemolytic ratio of QASAF-C12, QASAF-C14, QASAF-C16, and QASAF-C18; (B) Relative cell viability of Hep G2 incubated in medium containing different concentrations of QASAF nanofibers, and (C) cell morphology and survival status of QASAF and Hep G2 at 125 µg/mL.

morphology of Hep G2 cells in each group (Fig. 3C), while there is a significant change in the control group, further verifying the low toxicity of QASAF to cells and good biocompatibility.

3.2. *In vitro* and *in vivo* antimicrobial performance of QASAF against *S. aureus* infection

The antibacterial growth of QASAF against *S. aureus* is determined by an antibacterial growth curve and plate coating. All four QASAFs show strong bactericidal ability against *S. aureus*, positively correlated with dose (Fig. 4A). Among them, QASAF-C18 shows better antibacterial

performance. The antibacterial properties of QASAF are as follows: QASAF-C18 > QASAF-C16 > QASAF-C14 > QASAF-C12, suggesting that the longer the carbon chain of linear alkanes, the better the antibacterial properties against *S. aureus* (Zhang et al., 2016; Zhou et al., 2023).

When the concentrations are 25, 50, 75, and 150 µg/mL, QASAF-C18, QASAF-C16, QASAF-C14, and QASAF-C12 achieve 100 % sterilization (Fig. 4A). Moreover, QASAF-C18 exhibits the best antibacterial performance against *S. aureus*.

The minimum inhibitory concentration (MIC) of QASAF at different concentrations against *S. aureus* is determined by the CCK-8 kit (Yang et al., 2016), as shown in Table 2. The MIC values of QASAF-C12,

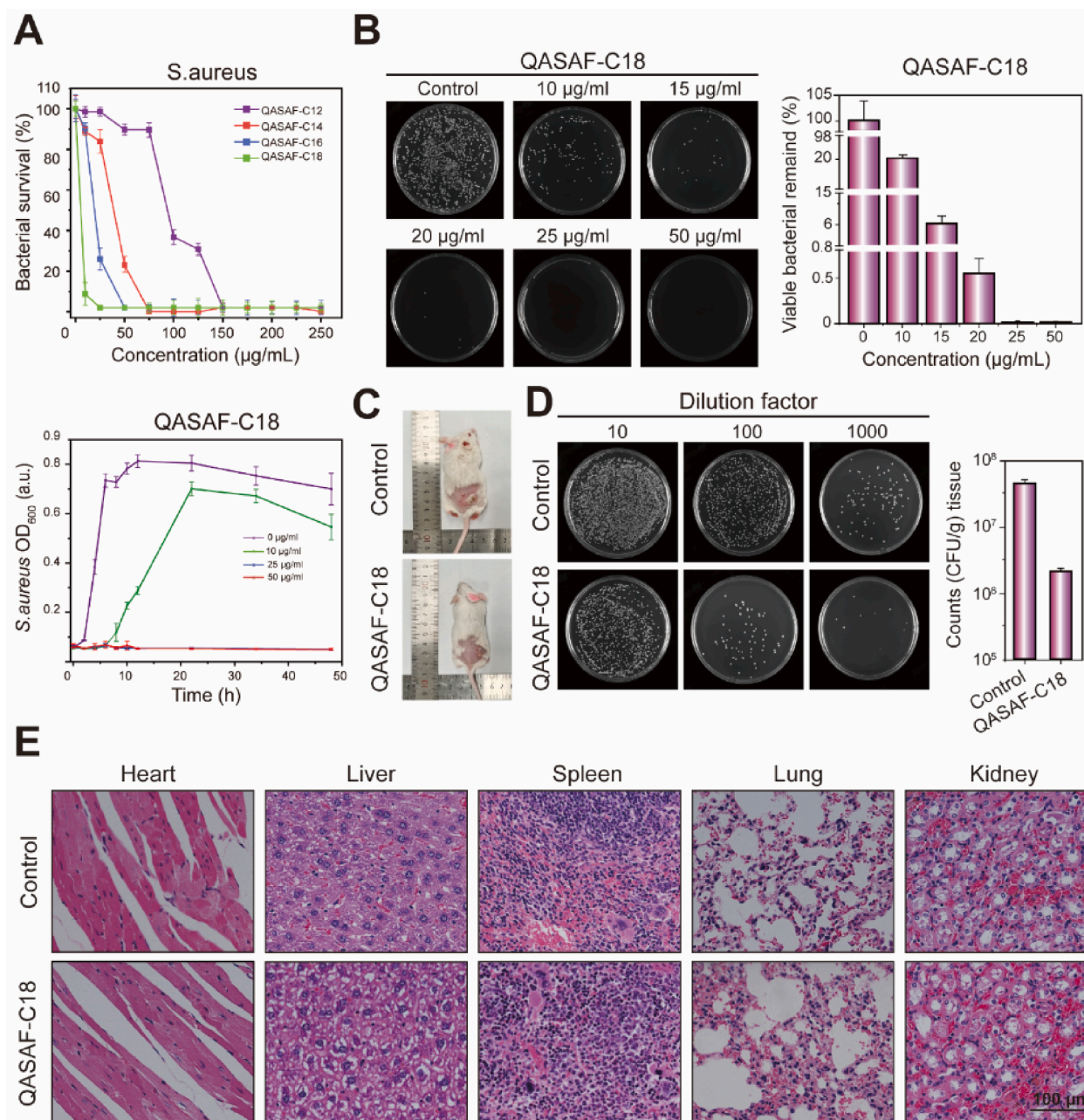


Fig. 4. (A) Bacterial survival after 10 h of co-culture of QASAF with *S. aureus* and growth kinetic curves of QASAF-C18 at different concentrations, (B) quantitative analysis of co-culture dilution coating at different concentrations of QASAF-C18 and *S. aureus* (C) subcutaneous injection of *S. aureus* and QASAF-C18 locus in mice, (D) quantitative analysis of tissue bacterial dilution smear, and (E) tissue sections of heart, liver, spleen, lung, and kidney. All data are presented as the means \pm SD ($n = 3$). (** $p < 0.01$). Bar = 10 μ m.

Table 2

MIC values of four QASAFs against *S. aureus* (μ g/mL).

Species	Gram type	Medicine	MIC [μ g mL ⁻¹]
<i>S. aureus</i>	G+	QASAF-C12	150
		QASAF-C14	75
		QASAF-C16	50
		QASAF-C18	25

QASAF-C14, QASAF-C16, and QASAF-C18 are 150, 75, 50, and 25 μ g/mL, respectively, consistent with the results obtained by the above antibacterial growth curve method, further verifying the antibacterial performance of QASAF-C18 against *S. aureus*.

The effects of QASAF-C18 concentration on *S. aureus* are further

evaluated. The relationship between optical density OD600 at 600 nm and time is also explored. The growth curve of QASAF-C18 against *S. aureus* is obtained (Fig. 4A). When the concentration is lower than 25 μ g/mL, the OD600 value of the QASAF-C18 group increases with time. After 24 h, the OD600 value decreased due to nutrition exhaustion and some bacterial colonies' death. The QASAF-C18 at 25 μ g/mL concentration completely suppresses the *S. aureus* growth within 48 h since OD600 of the bacterial solution at 600 nm is 0.

Fig. 4B shows the quantitative statistical analysis of antibacterial properties and the number of colonies at different concentrations of QASAF-C18 against *S. aureus* by a plate coating method. Compared with the control group, the QASAF-C18 concentration increased from 10 μ g/mL to 50 μ g/mL, and the bacterial colonies in LB agar plate culture dishes decreased significantly. However, sterile colonies are formed in

the culture dish when the concentration of QASAF-C18 is 25 $\mu\text{g/mL}$ and 50 $\mu\text{g/mL}$.

The antibacterial properties of QASAF-C18 *in vivo* are evaluated using a mice model of *S. aureus* subcutaneous infection. The subcutaneous injection of *S. aureus* and QASAF-C18 sites in mice is depicted in Fig. 4C. In the control group, the subcutaneous infection site is significantly more evident with pale white purulent tissue than in the QASAF-C18 group. The infection site of the subcutaneous injection of QASAF-

C18 is significantly improved at the infection site.

Fig. 4D indicates the number of bacterial colonies in the subcutaneously infected tissues of mice on day 5. The number of bacterial colonies at different concentration gradients of the QASAF-C18 group is lower than in the control group, revealing the excellent antibacterial effect of QASAF-C18 *in vivo*.

The pathological section results of the mouse heart, liver, spleen, lung, and kidney are shown in Fig. 4E. There are no obvious

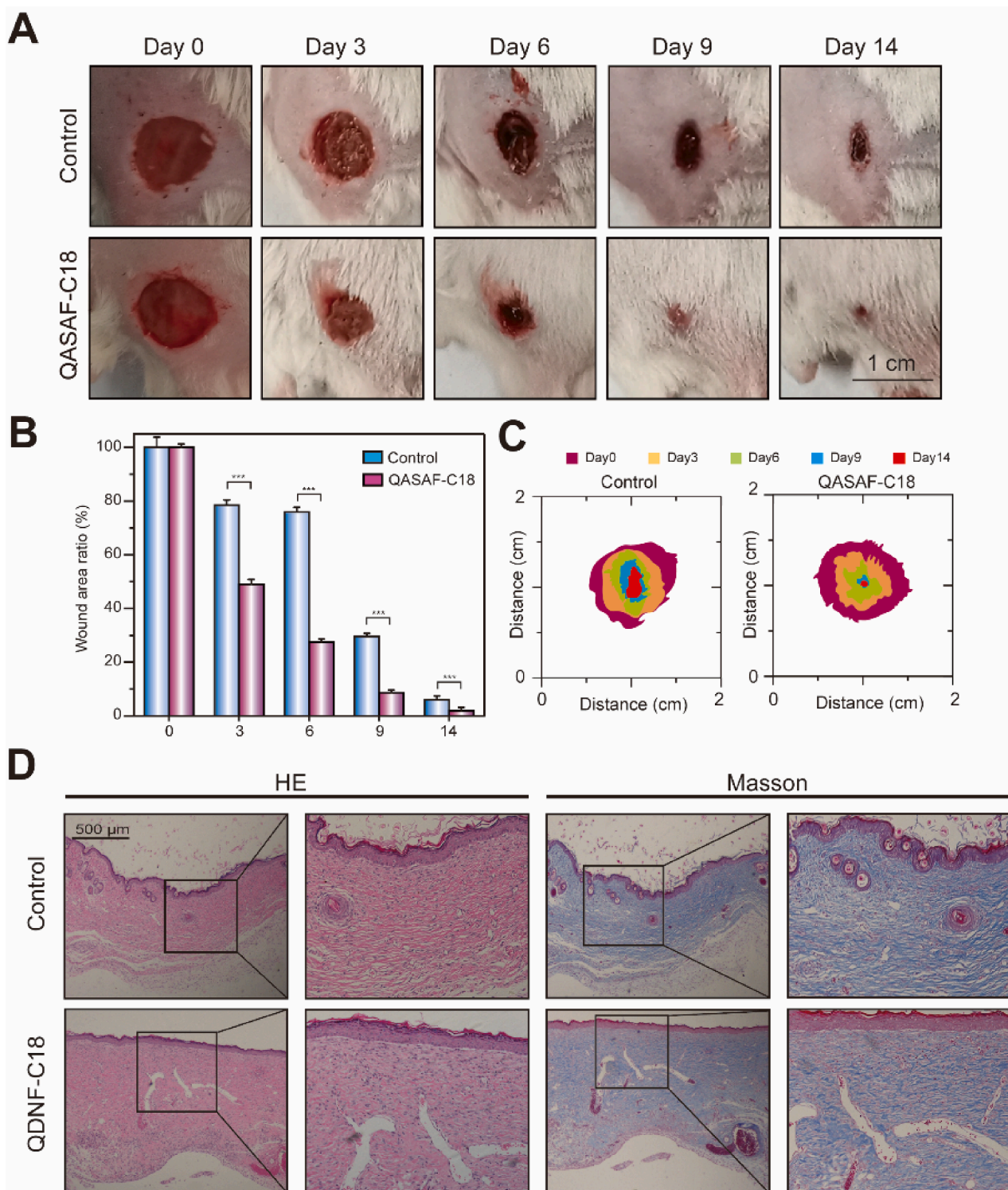


Fig. 5. (A) Wound healing, (B) wound healing ratio, and (C) wound healing area of QASAF-C18 treated mice. (D) Tissue section H&E and Masson staining of mouse epidermis in wound healing model. All data are presented as the means \pm SD ($n = 3$). (** $p < 0.01$). Bar = 500 μm .

abnormalities in the pathological sections of the heart, liver, spleen, lung, and kidney in the QASAF-C18 group, indicating that QASAF-C18 is injected subcutaneously without damaging the mice. These results suggest that QASAF-C18 has good biosafety.

3.3. Wound healing promoting effect of QASAF-C18

Mouse-infected wound model is used to evaluate the healing effect of QASAF-C18 on infected wounds. Compared with the control group, QASAF-C18 significantly promotes wound healing (Fig. 5A). The wounds in the QASAF-C18 group are scabbed on the 3rd day, and the wound area in mice is remarkably smaller than the other groups. The ratio of the healing area to the initial wound area at different time points

is shown in Fig. 5B. On day 14, there was still a large scab tissue in the control group; the wound area was 11.83 % of the initial wound area. In contrast, the wound area of the QASAF-C18 group is only 1.41 % of the initial wound area.

The visual statistics of wound healing trajectory and wound area size during the healing in mice at different time points are shown in Fig. 5C, which shows that the wound area in the QASAF-C18 group is smaller than the control group. Therefore, it is suggested that QASAF-C18 can kill the bacteria at the wound site, preventing the wound from inflammatory reactions triggered by the infection. Therefore, QASAF-C18 can promote the healing of infected wounds.

Finally, the pro-healing effect of QASAF-C18 is evaluated on infected wounds by pathological sections of traumatic tissue. H&E-stained and

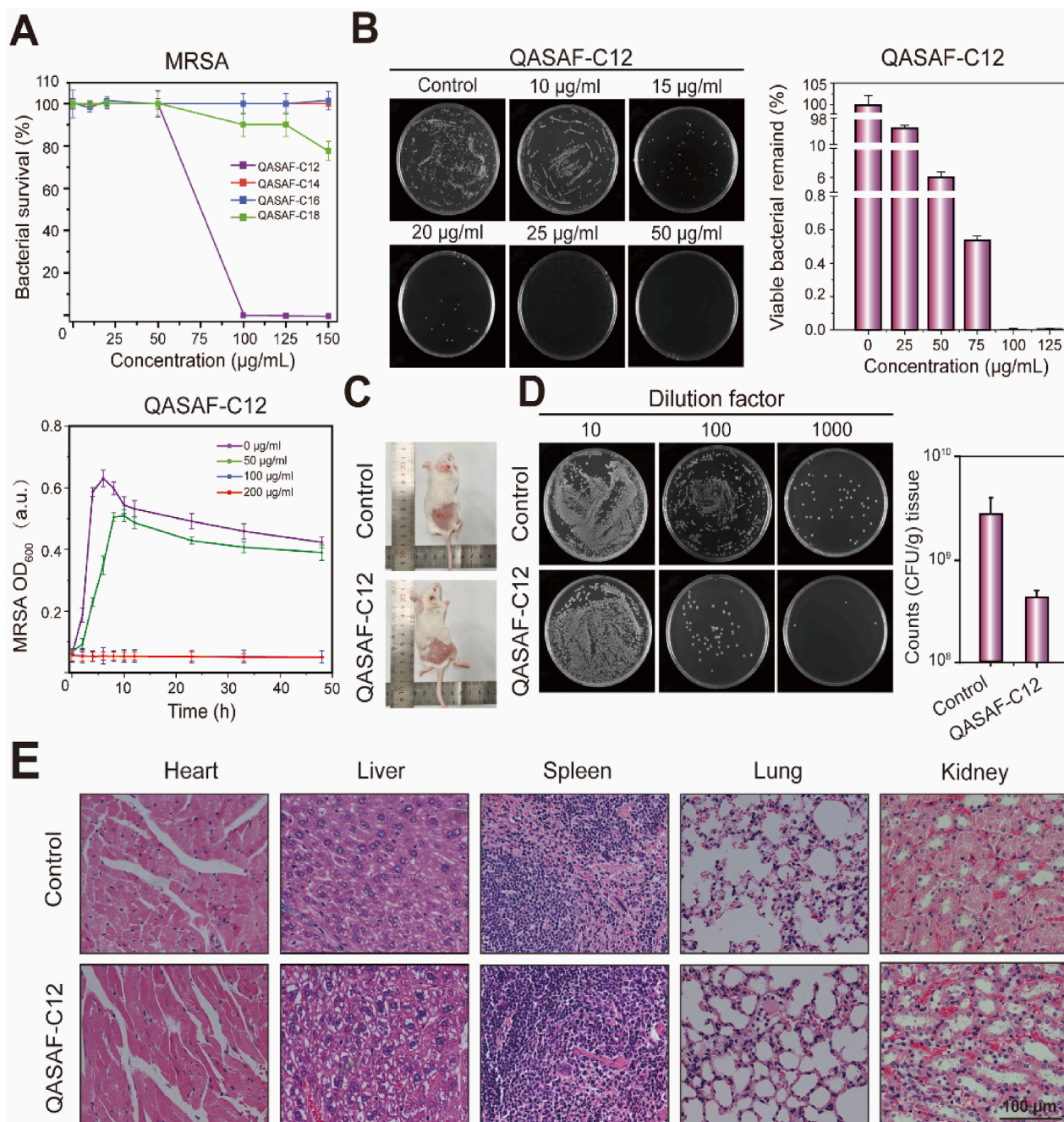


Fig. 6. (A) Bacterial survival after 10 h co-culture of QASAF-C12 with MRSA and kinetic growth curves, (B) tissue bacterial dilution smear observation and quantitative analysis, (C) mice subcutaneously injected with MRSA bacteria and QASAF-C12 locus, (D) tissue bacterial dilution smear observation and quantitative analysis, and (E) tissue sections of heart, liver, spleen, lung, and kidney of mice.

Masson-stained sections of the wound site are prepared on day 14. The QASAF-C18 group produced more inflammatory cells during wound healing. In addition, collagen shows blue color in Masson staining. The higher concentration of collagen deposited on the wound surface promotes healing. The QASAF-C18 group produces more collagen Masson protein than the control group, suggesting the pro-healing effect on infected wounds.

3.4. *In vitro* and *in vivo* antimicrobial performance of QASAF against MRSA

Fig. 6A indicates the antibacterial growth curve of QASAF against MRSA *in vitro*. Obtained results reveal that only QASAF-C12 exhibits the highest antibacterial performance against MRSA. The antibacterial activity against MRSA is as follows; QASAF-C12 > QASAF-C14 > QASAF-C16 > QASAF-C18. In addition, QASAF-C12 at a 100 µg/mL concentration achieves 100 % sterilization, while QASAF-C14, QASAF-C16, and QASAF-C18 cannot inhibit MRSA at the same concentration. Therefore, QASAF-C12 is selected as the best antibacterial fiber against MRSA.

The MIC of QASAFs' different concentrations against MRSA is determined using the CCK-8 kit (Table 3). The MIC value of QASAF-C12 is 100 µg/mL, indicating its inhibitory effect on MRSA at this concentration. The MIC values of QASAF-C14, QASAF-C16, and QASAF-C18 are all higher than 500 µg/mL with an inhibitory effect on MRSA. These results further indicate that QASAF-C12 exhibits the best antibacterial performance against MRSA.

The antibacterial performance of QASAF-C12 against MRSA is also evaluated by coating plate assay. The bacterial survival rate decreased significantly with the increase in concentration from 25 µg/mL to 125 µg/mL (Fig. 6B). The plate shows almost no MRSA when the concentration reaches 100 µg/mL. Quantitative analysis reveals that the antibacterial performance of the QASAF-C12 group is significantly higher than that of the control group. The bacterial survival rate in the QASAF-C12 group co-cultured with MRSA reaches almost 0 % at 100 µg/mL and 125 µg/mL concentrations. These results reveal that QASAF-C12 exhibits good antibacterial properties at this concentration.

A mouse model of MRSA subcutaneous infection is constructed, and the antibacterial properties of QASAF-C12 are evaluated *in vivo*. The infection site for the control group shows pale white purulent tissue, and the subcutaneous infection site for the QASAF-C12 group is significantly improved (Fig. 6C).

The subcutaneous infection sites of the two groups were collected for homogenate treatment and plate culture on the 5th day, and the number of bacterial colonies was calculated to evaluate the therapeutic effect. The number of bacterial colonies at different concentration gradients of the QASAF-C12 group was significantly lower than that in the control group, indicating an obvious antibacterial effect of QASAF-C12 *in vivo* (Fig. 6D).

After 5 days, both mice groups were dissected, and the heart, liver, spleen, lung, kidney, and other major organs were collected for pathological observation, and organ damage after subcutaneous injection of QASAF-C12 was obtained. No obvious abnormalities are detected in the pathological sections of the main organs in the QASAF-C12 treated group (Fig. 6E), suggesting that QASAF-C12 is injected subcutaneously into the body without causing damage to mice and QASAF-C12 exhibits good biocompatibility.

Table 3
MIC values of four QASAFs against MRSA (µg/mL).

Species	Gram type	Medicine	MIC [µg mL ⁻¹]
MRSA	G+	QASAF-C12	100
		QASAF-C14	>500
		QASAF-C16	>500
		QASAF C18	>500

3.5. Effect of QASAF-C12 in promoting wound healing in MRSA infected wound

Fig. 7 shows the healing-promoting effect of QASAF-C12 on MRSA-infected wounds. The ratio of the infected wound healing area to the initial infected wound area at different time points is determined. Compared with the control group, QASAF-C12 exhibits a significant wound healing-promoting effect, as shown in Fig. 7A. The wounds treated with QASAF-C12 crusted over on day 3 after treatment, significantly smaller than that of the control group. On day 14, the wound was healed, and the trauma area was only 1.93 % of the initial wound area. For the control group, the wound still had large scabs of tissue, and the wound area was 6.00 % of the initial trauma area (Fig. 7B). These results show that QASAF-C12 has a significant pro-healing effect on MRSA-infected wounds.

Fig. 7C and 7D show the visual statistics of wound healing trajectory and area size during infected wound healing. The wound area in the QASAF-C12 group is significantly smaller than the control group at different time points (Fig. 7C). QASAF-C12 promptly killed bacteria at infected wound sites to promote healing. Therefore, it can be concluded that QASAF-C12 can promote the healing in infected wounds.

On day 14, wound site tissues were made into H&E-stained and Masson-stained sections to assess the pro-healing effect of QASAF-C12 (Fig. 7D). The results suggest that control and QASAF-C12 groups produce more inflammatory cells during wound healing. The number of inflammatory cells in the QASAF-C12 group is lower than in the control group, indicating that QASAF-C12 could kill the bacteria on the wound surface, thereby avoiding the inflammatory reaction. Masson staining results suggest that the QASAF-C12 group produces more collagen in the wound than the control group, further verifying the pro-healing effect of QASAF-C12.

4. Discussion

One of the primary challenges in the development of innovative QAS antimicrobial materials lies in improving blood compatibility and biosafety (Jiao et al., 2017) (Wang et al., 2023). In this investigation, by harnessing the advantageous properties of Dextran to enhance both hemocompatibility and biocompatibility, QAS compounds were synthesized with Dextran to produce four distinct QASAF variants: QASAF-C12, QASAF-C14, QASAF-C16, and QASAF-C18. The results revealed that QASAF concentrations ranging from 25-125 µg/mL exhibited cellular non-toxicity and demonstrated admirable hemocompatibility and biosafety. Particularly, QASAF-C18 exhibited exceptional antibacterial effectiveness against *S. aureus* and demonstrated a notable wound healing promotion effect in murine models. In parallel, QASAF-C12 displayed remarkable antibacterial efficacy against MRSA and also exhibited a significant wound healing promotion effect in mice. The successful creation of QASAF serves as a valuable guide for the development of antibacterial wound dressings.

Both human and mammalian cells possess negatively charged surfaces, and the presence of positively charged cationic quaternary ammonium compounds can lead to varying degrees of damage to these structures in anionic organisms. The assessment of hemolysis rate serves as a crucial parameter in evaluating the biocompatibility of biological materials. As per the guidelines set by the American Society for Testing and Materials (ASTM F756-00, 2000) (Hajji et al., 2019), a hemolysis rate exceeding 5 % signifies hemolysis, while rates between 2-5 % are categorized as mild hemolysis, and rates below 2 % are deemed non-hemolytic. Notably, the experimental data from this study depicted that the hemolysis rate of QASAF remained below 5 % across all effective inhibitory concentration ranges, with minimal hemolytic activity observed at higher concentrations, indicating excellent hemocompatibility.

Zhou et al. introduced a novel antibacterial material (DMAEMA-PMDPM), with cytotoxicity assay results revealing a cell survival rate

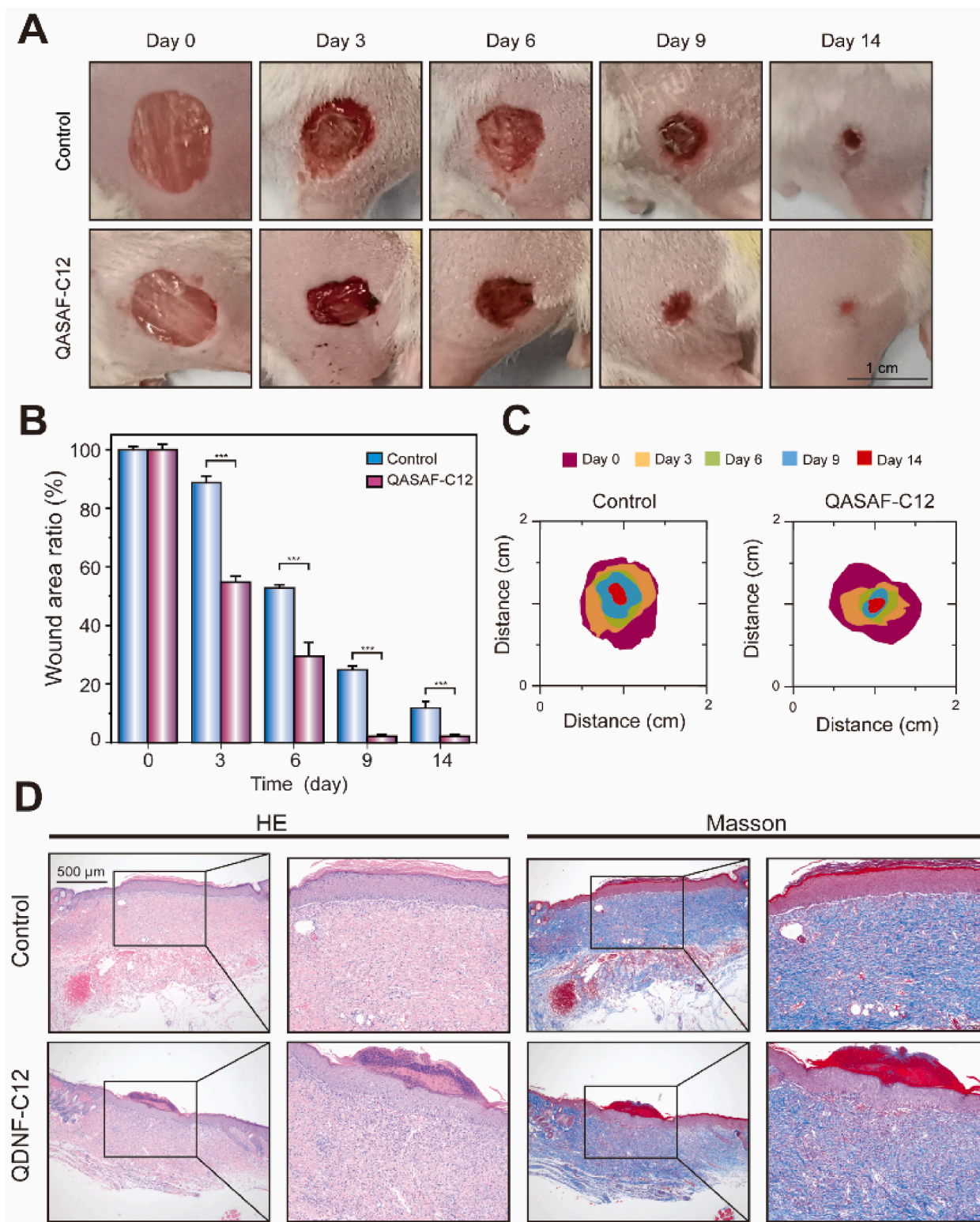


Fig. 7. (A) Wound healing, (B) wound healing ratio, and (C) wound healing area of mice in the wound healing model. (D) Tissue section H&E and Masson staining of mouse epidermis in wound healing model. All data are presented as the means \pm SD ($n = 3$). (** $p < 0.01$). Bar = 500 μ m.

exceeding 85%. In a separate study by Ye *et al.* in 2016, antimicrobial materials GO-1227 and GO-CPB were developed by assembly of dodecylmethylbenzylammonium chloride (1227) and cetyl pyridine bromide (CPB) on graphene oxide (GO) surfaces. Notably, the cytotoxicity levels of GO-1227 and GO-CPB were significantly lower compared to their intermediate counterparts, yielding cell survival rates of 78.7%

and 77.9%, respectively. Moreover, in 2017, Zhang *et al.* engineered a cross-linked waterborne polyurethane (CPTMGPU) exhibiting long-term stability by leveraging gemini quaternary ammonium salt (GQAS) as a key component. The cell viability assays revealed a substantial increase in cell survival rate compared to the latex rubber extract employed as a positive control, with a rate of 89%. These outcomes underscored the

favorable morphology and growth status of Hep G2 cells within the QASAF group, showcasing a cell survival rate exceeding 85 %. This underscores the minimal cytotoxicity and robust biosafety profile exhibited by QASAF.

In 2022, Roy *et al.* prepared quaternary ammonium-substituted branched-chain starch (CP) derivatives with glycidyl-trimethylammonium chloride (GTMAC)/branched-chain starch mass ratios ranging from 10 to 20, named CP-1, CP-2, CP-3, and CP-4 (Roy *et al.*, 2022). Among the derivatives, the antibacterial activity was found to follow the order CP-4 > CP-3 > CP-2 > CP-1. In particular, CP-4 completely killed *S. aureus* at doses of > 4 $\mu\text{g mL}^{-1}$. Song *et al.* synthesized long-chain polymeric organic bisquaternary ammonium salts (BQAS) with broad-spectrum bactericidal activity (Zhiyong *et al.*, 2018). The obtained BQAS growth curves suggested that the longer the length of the straight alkane carbon chain, the better the antibacterial performance in BQAS with different carbon chain lengths. The *in vitro* and *in vivo* results of this study were consistent with those reported by the above studies, in that the longer the length of the straight alkane carbon chain, the better the antibacterial performance of QASAF with different carbon chain lengths against *S. aureus*. Among them, QASAF-C18 exhibited the best antibacterial performance against *S. aureus*.

In the year 2016, Zhang and colleagues meticulously engineered a series of quaternized luminescent silicon nanoparticles (SiNPs) (Zhang *et al.*, 2016). Through meticulous agar plate counting experiments, it was deduced that a concentration of 10 $\mu\text{g/ml}$ of SiNPs-C18 could effectively eliminate *S. aureus*. In a separate investigation, Liu *et al.* synthesized graphene oxide-quaternary ammonium salt composites (GO-QAS) with exceptional *in vitro* antimicrobial efficacy, as demonstrated by nearly complete eradication of *S. aureus* at a concentration of 200 $\mu\text{g/mL}$ (Liu *et al.*, 2018). Lei *et al.* innovatively developed a range of glycidyl trimethyl ammonium chloride-grafted chitosan (QCS)/aldehyde-dextran (ODex) Schiff base hydrogels, elegantly named QCS-ODex (Nie *et al.*, 2023). Their research unveiled that QCS-ODex exhibited a notable antibacterial activity of 60 % against *S. aureus*. Our findings closely mirror the outcomes observed in the aforementioned studies. Our agar plate counting results further showcased the potent antimicrobial properties of 25 $\mu\text{g/mL}$ of QASAF-C18 against *S. aureus* and 100 $\mu\text{g/mL}$ of QASAF-C12 against MRSA, with no colonies detected in the dishes. Furthermore, the results indicated that QASAF-C18 displayed robust antimicrobial efficacy against *S. aureus*, while QASAF-C12 exhibited formidable antimicrobial activity against MRSA.

Song *et al.* adeptly synthesized a high molecular weight polymeric organic BQAS with broad-spectrum bactericidal capabilities, demonstrating a minimal inhibitory concentration (MIC) ranging from 8-32 $\mu\text{g/ml}$ against *S. aureus* (Song *et al.*, 2018). Zhao and colleagues meticulously prepared the antimicrobial compound QCS-EDA-CDs, showcasing superior antimicrobial performance against *S. aureus* with an MIC exceeding 500 $\mu\text{g/ml}$ (Zhao *et al.*, 2022). In our current study, MIC values of 25 $\mu\text{g/mL}$ for QASAF-C18 against *S. aureus* and 100 $\mu\text{g/mL}$ for QASAF-C12 against MRSA were determined, both exhibiting admirably low values. Overall, the MIC results unequivocally emphasize the unmatched inhibitory power of QASAF-C18 against *S. aureus*, while highlighting the superior inhibitory performance of QASAF-C12 against MRSA.

In the year 2022, Yu *et al.* innovated a hydrogel possessing antibacterial, hemostatic, self-healing, and injectable properties known as oxidized quaternized guar gum @carboxymethyl chitosan (OQGG@CMCS), which demonstrated the ability to enhance the recovery of wounds infected with *S. aureus* (Yu *et al.*, 2022). Notably, the group treated with OQGG@CMCS hydrogel exhibited accelerated wound healing during the course of the study. By day 9, the wound exhibited reduced size, a thicker epidermal layer, well-developed appendages, and diminished inflammatory cells compared to the control group. By day 14, remarkable progress towards complete healing was observed. Furthermore, Roy *et al.* explored the pro-wound healing potential of CP40 following the successful validation of the excellent

antimicrobial properties of CP-1, CP-2, CP-3, and CP-4 (Roy *et al.*, 2022). Within a mere 7 days post-surgery, the CP-4 group displayed a remarkable increase in healing rate from 20 % to 60 %, achieving complete healing within 12 days. These findings underscore the significant impact of CP-4 in promoting wound healing in *S. aureus*-infected wounds. In a similar vein, the research by Liu *et al.* shed light on the profound ability of GO-QAS in advancing wound healing in *S. aureus*-infected wounds (Liu *et al.*, 2018). At day 3 post-surgery, conspicuous absence of purulent discharge was noted in the GO-QAS group as opposed to the control group. By day 7 post-surgery, the percentage of closed wounds in the various groups including blank, control, GO, and GO-QAS stood at 78.7 %, 58.9 %, 66.4 %, and 77.2 %, respectively. Our *in vivo* investigations align closely with the aforementioned studies, revealing that QASAF-C18 exhibited notable wound healing efficacy in wounds of *S. aureus*-infected mice, while QASAF-C12 showcased remarkable healing effects in wounds of MRSA-infected mice.

In essence, our inquiry validates the hypothesis that the fusion of antimicrobial agents within a dextran matrix, achieved through covalent bonding with QAS, augments the hemocompatibility, biocompatibility, and antimicrobial potency of QAS-derived antimicrobial materials. Consequently, the development of QASAF-C18 and QASAF-C12 in this research serves as a valuable reference for the advancement of antibacterial wound dressings.

CRedit authorship contribution statement

Guangyu Pan: Data curation, Formal analysis, Methodology, Project administration. **Qin Wang:** Conceptualization, Data curation, Formal analysis, Investigation, Visualization, Writing – original draft. **Hangxing Ding:** Conceptualization, Data curation, Formal analysis, Resources, Writing – original draft, Writing – review & editing. **Jianbin Deng:** Data curation, Investigation. **Shiqi Gao:** Data curation, Formal analysis, Validation. **Liping Wang:** Funding acquisition, Investigation, Supervision, Writing – original draft, Writing – review & editing.

Declaration of competing interest

The authors declare that they have no known competing financial interests or personal relationships that could have appeared to influence the work reported in this paper.

Acknowledgements

This work was supported by the National Natural Science Foundation of China (52265042), Guangxi Scholar Grant (30501020001), the Guangxi Natural Science Foundation (2021AC19246, 2020GXNSFAA159033), Guangxi National Health Commission Program (Z20210381, Z20210735), the Guangxi Science and Technology Base and Talent Project (GuikeAD20238051).

Appendix A. Supplementary material

Supplementary data to this article can be found online at <https://doi.org/10.1016/j.arabjc.2024.105771>.

References

- Alexandre, N., Ribeiro, J., Gärtner, A., *et al.*, 2014. Biocompatibility and hemocompatibility of polyvinyl alcohol hydrogel used for vascular grafting—*In vitro* and *in vivo* studies. *J. Biomed. Mater. Res. A* 102, 4262–4275.
- Becker, K., Schaumburg, F., Fegeler, C., *et al.*, 2017. *Staphylococcus aureus* from the German general population is highly diverse. *Int. J. Med. Microbiol. Ijmm* 307, 21.
- Brumfit, W., Hamilton-Miller, J., 1989. Methicillin-resistant *Staphylococcus aureus*. *N. Engl. J. Med.* 320, 1188–1196.
- C., W., 2017. Drug-resistant bacteria ranked. *Nature.* 543(7643): 15.
- Choi, H., Chatterjee, P., Lichtfouse, E., *et al.*, 2021. Classical and alternative disinfection strategies to control the COVID-19 virus in healthcare facilities: a review. *Environ. Chem. Lett.* 19, 1945–1951.

- Del Bino, L., Østerlid, K.E., Wu, D.-Y., et al., 2022. Synthetic glycans to improve current glycoconjugate vaccines and fight antimicrobial resistance. *Chem. Rev.* 122, 15672–15716.
- Deng, X., Huang, B., Wang, Q., et al., 2021. A mussel-inspired antibacterial hydrogel with high cell affinity, toughness, self-healing, and recycling properties for wound healing. *ACS Sustain. Chem. Eng.* 9, 3070–3082.
- Diven, D.G., Pohl, J., Motamedi, M., 1996. Dye-enhanced diode laser photothermal ablation of skin. *J. Am. Acad. Dermatol.* 35, 211–215.
- Ferrer, M.C.C., Eckmann, U.N., Composto, R.J., et al., 2013. Hemocompatibility and biocompatibility of antibacterial biomimetic hybrid films. *Toxicol. Appl. Pharmacol.* 272, 703–712.
- Gharibi, R., Kazemi, S., Yeganeh, H., et al., 2019. Utilizing dextran to improve hemocompatibility of antimicrobial wound dressings with embedded quaternary ammonium salts. *Int. J. Biol. Macromol.* 131, 1044–1056.
- Gottenbos, B., van der Mei, H.C., Klatter, F., et al., 2002. In vitro and in vivo antimicrobial activity of covalently coupled quaternary ammonium silane coatings on silicone rubber. *Biomaterials* 23, 1417–1423.
- Guan, G., Lv, Q., Liu, S., et al., 2022. 3D-bioprinted peptide coupling patches for wound healing. *Mater. Today Bio* 13, 100188.
- Hajji, S., Khedir, S.B., Hamza-Mnif, I., et al., 2019. Biomedical potential of chitosan-silver nanoparticles with special reference to antioxidant, antibacterial, hemolytic and in vivo cutaneous wound healing effects. *Biochim. Biophys. Acta (BBA)-Gen. Subj.* 1863, 241–254.
- Jiang, Y.-W., Gao, G., Zhang, X., et al., 2017. Antimicrobial carbon nanospheres. *Nanoscale* 9, 15786–15795.
- Jiao, Y., Niu, L.-N., Ma, S., et al., 2017. Quaternary ammonium-based biomedical materials: State-of-the-art, toxicological aspects and antimicrobial resistance. *Prog. Polym. Sci.* 71, 53–90.
- Lee, H., Kim, S., Ryu, C., et al., 2020. Photothermal polymerization using graphene oxide for robust hydrogelation with various light sources. *ACS Biomater. Sci. Eng.* 6, 1931–1939.
- Linsley, C.S., Quach, V.Y., Agrawal, G., et al., 2015. Visible light and near-infrared-responsive chromophores for drug delivery-on-demand applications. *Drug Deliv. Transl. Res.* 5, 611–624.
- Liu, T., Liu, Y., Liu, M., et al., 2018. Synthesis of graphene oxide-quaternary ammonium nanocomposite with synergistic antibacterial activity to promote infected wound healing. *Burns Trauma* 6, 16. <https://doi.org/10.1186/s41038-018-0115-2>.
- Mann, R., Mitsidis, D., Xie, Z., et al., 2021. Antibacterial activity of reduced graphene oxide. *J. Nanomater.* 2021, 1–10.
- Minozzi, S., Pifferi, S., Brazzi, L., et al., 2021. Topical antibiotic prophylaxis to reduce respiratory tract infections and mortality in adults receiving mechanical ventilation. *Cochrane Database Systemat. Rev.* 1.
- Neu, B., Wenby, R., Meiselman, H.J., 2008. Effects of dextran molecular weight on red blood cell aggregation. *Biophys. J.* 95, 3059–3065.
- Nie, L., Wei, Q., Sun, M., et al., 2023. Injectable, self-healing, transparent, and antibacterial hydrogels based on chitosan and dextran for wound dressings. *Int. J. Biol. Macromol.* 233, 123494 <https://doi.org/10.1016/j.ijbiomac.2023.123494>.
- Pérez, L., Pinazo, A., García, M.T., et al., 2009. Cationic surfactants from lysine: Synthesis, micellization and biological evaluation. *Eur. J. Med. Chem.* 44, 1884–1892.
- Qi, K., Xing, X., Zada, A., et al., 2020. Transition metal doped ZnO nanoparticles with enhanced photocatalytic and antibacterial performances: experimental and DFT studies. *Ceram. Int.* 46, 1494–1502.
- Qian, W., Yan, C., He, D., et al., 2018. pH-triggered charge-reversible of glycol chitosan conjugated carboxyl graphene for enhancing photothermal ablation of focal infection. *Acta Biomater.* 69, 256–264.
- Qiao, Y., Ping, Y., Zhang, H., et al., 2019. Laser-activatable CuS nanodots to treat multidrug-resistant bacteria and release copper ion to accelerate healing of infected chronic nonhealing wounds. *ACS Appl. Mater. Interfaces* 11, 3809–3822.
- Rajkowska, K., Koziróg, A., Otlewska, A., et al., 2016. Quaternary ammonium biocides as antimicrobial agents protecting historical wood and brick. *Acta Biochim. Pol.* 63, 153–159.
- Roy, S., Kumari, M., Haloi, P., et al., 2022. Quaternary ammonium substituted pullulan accelerates wound healing and disinfects *Staphylococcus aureus* infected wounds in mouse through an atypical 'non-pore forming' pathway of bacterial membrane disruption. *Biomater. Sci.* 10, 581–601. <https://doi.org/10.1039/d1bm01542g>.
- Saidin, S., Jumat, M.A., Amin, N.A.A.M., et al., 2021. Organic and inorganic antibacterial approaches in combating bacterial infection for biomedical application. *Mater. Sci. Eng. C* 118, 111382.
- Shen, M., Forghani, F., Kong, X., et al., 2020. Antibacterial applications of metal-organic frameworks and their composites. *Compr. Rev. Food Sci. Food Saf.* 19, 1397–1419.
- Song, Z., Wang, H., Wu, Y., et al., 2018. Fabrication of bis-quaternary ammonium salt as an efficient bactericidal weapon against *Escherichia coli* and *Staphylococcus aureus*. *ACS Omega* 3, 14517–14525. <https://doi.org/10.1021/acso.3b01265>.
- Sun, X., Li, L., Zhang, H., et al., 2021. Near-infrared light-regulated drug-food homologous bioactive molecules and photothermal collaborative precise antibacterial therapy nanoplatfrom with controlled release property. *Adv. Healthc. Mater.* 10, 2100546.
- Usman, A., Zia, K.M., Zuber, M., et al., 2016. Chitin and chitosan based polyurethanes: A review of recent advances and prospective biomedical applications. *Int. J. Biol. Macromol.* 86, 630–645.
- Vereshchagin, A.N., Frolov, N.A., Egorova, K.S., et al., 2021. Quaternary ammonium compounds (QACs) and ionic liquids (ILs) as biocides: From simple antiseptics to tunable antimicrobials. *Int. J. Mol. Sci.* 22, 6793.
- Wang, L., Zhang, X., Zhang, X., et al., 2023. Mechanism analysis of a novel natural cationic modified dextran flocculant and its application in the treatment of blue algal blooms. *Int. J. Biol. Macromol.* 254, 128002 <https://doi.org/10.1016/j.ijbiomac.2023.128002>.
- Wangpaiboon, K., Waiyaseesang, N., Panpetch, P., et al., 2020. Characterisation of insoluble α -1, 3-/ α -1, 6 mixed linkage glucan produced in addition to soluble α -1, 6-linked dextran by glucansucrase (DEX-N) from *Leuconostoc citreum* ABK-1. *Int. J. Biol. Macromol.* 152, 473–482.
- Wiarachai, O., Thongchul, N., Kiatkamjornwong, S., et al., 2012. Surface-quaternized chitosan particles as an alternative and effective organic antibacterial material. *Colloids Surf. B Biointerfaces* 92, 121–129.
- Xi, G., Liu, W., Chen, M., et al., 2019. Polysaccharide-based lotus seedpod surface-like porous microsphere with precise and controllable micromorphology for ultrarapid hemostasis. *ACS Appl. Mater. Interfaces* 11, 46558–46571. <https://doi.org/10.1021/acsami.9b17543>.
- Xu, Q., Ji, Y., Sun, Q., et al., 2019. Fabrication of cellulose nanocrystal/chitosan hydrogel for controlled drug release. *Nanomaterials* 9, 253.
- Yang, J., Zhang, X., Ma, Y.-H., et al., 2016. Carbon dot-based platform for simultaneous bacterial distinguishment and antibacterial applications. *ACS Appl. Mater. Interfaces* 8, 32170–32181.
- Yu, X., Cheng, C., Peng, X., et al., 2022. A self-healing and injectable oxidized quaternized guar gum/carboxymethyl chitosan hydrogel with efficient hemostatic and antibacterial properties for wound dressing. *Colloids Surf. B Biointerfaces* 209, 112207.
- Yu, X., C. Cheng, X. Peng, et al., 2022. A self-healing and injectable oxidized quaternized guar gum/carboxymethyl chitosan hydrogel with efficient hemostatic and antibacterial properties for wound dressing. *Colloids Surf B Biointerfaces* 209, 112207. <https://doi.org/10.1016/j.colsurfb.2021.112207>.
- Yuan, Z., Tao, B., He, Y., et al., 2019. Biocompatible MoS₂/PDA-RGD coating on titanium implant with antibacterial property via intrinsic ROS-independent oxidative stress and NIR irradiation. *Biomaterials* 217, 119290.
- Zeerleder, S., Mauron, T., Lämmle, B., et al., 2002. Effect of low-molecular weight dextran sulfate on coagulation and platelet function tests. *Thromb. Res.* 105, 441–446.
- Zhang, X., Chen, X., Yang, J., et al., 2016. Quaternized silicon nanoparticles with polarity-sensitive fluorescence for selectively imaging and killing gram-positive bacteria. *Adv. Funct. Mater.* 26, 5958–5970. <https://doi.org/10.1002/adfm.201602185>.
- Zhang, X., X. Chen, J. Yang, et al., 2016. Quaternized Silicon Nanoparticles with Polarity-Sensitive Fluorescence for Selectively Imaging and Killing Gram-Positive Bacteria. *Advanced Functional Materials* 26, 5958–5970.
- Zhao, D., Zhang, R., Liu, X., et al., 2022. Screening of chitosan derivatives-carbon dots based on antibacterial activity and application in anti-*Staphylococcus aureus* biofilm. *Int. J. Nanomed.* 17, 937–952. <https://doi.org/10.2147/ijn.S350739>.
- Zhao, C., Zhou, L., Chiao, M., et al., 2020. Antibacterial hydrogel coating: Strategies in surface chemistry. *Adv. Colloid Interface Sci.* 285, 102280.
- Zhiyong, Song, Huajuan, et al., 2018. Fabrication of Bis-Quaternary Ammonium Salt as an Efficient Bactericidal Weapon Against *Escherichia coli* and *Staphylococcus aureus*. *ACS omega* 3, 14517–14525.
- Zhou, Z., Li, B., Liu, X., et al., 2021. Recent progress in photocatalytic antibacterial. *ACS Appl. Bio Mater.* 4, 3909–3936.
- Zhou, Z., Zhou, S., Zhang, X., et al., 2023. Quaternary ammonium salts: Insights into synthesis and new directions in antibacterial applications. *Bioconjug. Chem.* 34, 302–325.